Iranian Journal of Pharmaceutical Sciences
2024: 20 (4): 293- 314
https://journals.sbmu.ac.ir/IJPS

Original Article

Identification of Aquaporin 3 Inhibitors from *Santalum album* Phytochemicals for Melanoma treatment: A Computational Study

Mudassir Alam[a*], Kashif Abbas[a], Mohd Tanjeem Raza[a], S Mohd Hasan Abedi[a], Hafsa Haq[a], Mohd Mustafa[b]

[a]*Faculty of Life Sciences, Department of Zoology, Aligarh Muslim University, Aligarh, 202002, India,* [b]*Department of Biochemistry, JN Medical College, Aligarh Muslim University, Aligarh, 202002, India*.

Abstract

This study employed a multifaceted computational approach to identify potential inhibitors of aquaporin 3 (AQP3) derived from phytochemicals found in the *Santalum album* as potential drug candidates for melanoma treatment. Initially, the AQP3 structure was modeled using SWISSMODEL, which yielded a satisfactory GMQE score of 0.70 and a MolProbity score of 1.61. The QMEAN Z-score (-3.29) indicated acceptable quality, and Ramachandran analysis revealed that 95.12% of the residues were within the favored region. Virtual screening of phytochemicals utilized AutoDock Vina to identify compounds with strong binding affinity for AQP3. Phytochemicals exhibiting docking scores of -7 or less were selected for further analysis. The physicochemical properties and drug-likeness were evaluated using SWISS ADME, revealing compounds with favorable solubility, permeability, and gastrointestinal absorption. Biological activity prediction through the PASS web server indicated significant probabilities of dermatologic and antineoplastic activities for selected compounds. ADME/T properties were analyzed using the ADMET Lab 2.0 server, demonstrating favorable pharmacokinetic characteristics and safety profiles for compounds such as alpha-bergamotenol, himachalol, lupeol, levomenol, and sclareol. Except for himachalol, the other phytochemicals showed good safety profiles. Apart from himachalol, the remaining phytochemicals demonstrated favorable safety profiles. Molecular dynamics (MD) simulations provided insights into the stability and flexibility of receptor-ligand complexes over time, with compounds such as sclareol and levomenol exhibiting stable interactions. This comprehensive computational investigation highlights the potential of phytochemicals from *S. album*, particularly levomenol and sclareol, as inhibitors of AQP3. Further experimental validation is necessary to explore their clinical application in treating dermatologic conditions and cancer.

Keywords: Melanoma, Sandalwood, Aquaporins, MD simulation, Sclareol, Levomenol.

Corresponding Author: Mudassir Alam; Faculty of Life Sciences, Department of Zoology, Aligarh Muslim University, Aligarh, INDIA 202002. E-mail: gh7949@myamu.ac.in

Cite this article as: Alam M, Abbas K, Raza MT, Abedi SMH, Haq H, Mustafa M. *Identification of Aquaporin 3 Inhibitors from Santalum album Phytochemicals for Melanoma treatment: A Computational Study*. J. Pharm. Sci., 2024, 20 (4): 293- 314.

DOI: https://doi.org/10.22037/ijps.v20i4.44925

1. Introduction

1.1. Melanoma and Skin Cancer: A Global Health Challenge

Melanoma, a form of skin cancer, poses a significant global health concern. In 2020, an estimated 324,635 new cases and 57,043

deaths due to melanoma were reported worldwide [1]. The incidence rates of melanoma have steadily increased over the past few decades, making it one of the most rapidly increasing cancers in many parts of the world [2].

Cutaneous malignancies constitute a spectrum of neoplasms, including basal cell carcinomas (BCCs), squamous cell carcinomas (SCCs), and malignant melanomas [3]. SCC and BCC are classified as non-melanoma skin cancers (NMSCs), distinct from the more aggressive and potentially metastatic malignant melanoma [4].

1.2. Aquaporins and Their Role in Cancer

Aquaporins (AQPs) are transmembrane protein complexes facilitating the transport of selective water and small solutes across cell membranes. They are composed of four identical subunits, with each monomer forming a pore that selectively allows the passage of water molecules [5]. AQPs are categorized into orthodox aquaporins, specifically water transport, and aquaglyceroporins, which also allow the passage of small solutes like glycerol [6]. Among the recognized AQP isoforms, AQP1 (present in endothelial cells) and AQP3 (present in the basal layer of human keratinocytes) have been extensively studied in cancer research [7]. AQP3, in particular, has attracted increased attention due to its abundant expression in the skin and strong association with melanoma [8].

1.3. AQP3 and Its Role in Cancer Progression

The overexpression of AQP3, a water/glycerol channel, has been linked to increased glycerol uptake, facilitating tumor growth, angiogenesis, and metastasis [15]. In addition to melanoma, AQP3 is overexpressed in various other cancers, including lung [16, 17], colon [18], esophageal and oral squamous cell carcinoma [19], and hepatocellular carcinoma [20]. One of the mechanisms by which AQP3 contributes to cancer progression is by facilitating the transport of hydrogen peroxide (H^2O^2) across cellular membranes [24]. This influx of H^2O^2 potentiates the phosphorylation and activation of crucial signaling kinases, such as Akt and Erk [25], which are involved in cell proliferation and survival. Additionally, AQP3 overexpression upregulates the expression and activity of matrix metalloproteases (MMPs), contributing to cancer cells' increased invasiveness and metastatic potential by degrading tissue barriers [26]. Furthermore, the facilitated transport of glycerol mediated by AQP3 generates ATP, promoting the growth and survival of tumor cells. Targeting the expression of AQP3 can attenuate intracellular signaling cascades, such as MAPK, PI3K/Akt, Wnt/β-catenin, and Notch signaling pathways, leading to reduced cell proliferation, migration, and invasion [28].

1.4. Potential of Natural Compounds as AQP3 Inhibitors

Inorganic compounds containing metals like mercury, silver, and gold have shown potential as selective inhibitors of AQPs [29]. Subsequent studies have explored the inhibitory potential of metal-based drugs, including those used for rheumatic, cancer, and antibacterial therapies, against AQP1 and AQP3, yielding promising results [30]. Efforts have also been

made to characterize and synthesize gold-based compounds as novel AQP3 inhibitors [31, 32]. However, the use of metal-based compounds as AQP3 inhibitors may be associated with potential toxicity concerns. Therefore, exploring natural compounds as AQP3 inhibitors could offer a safer and more effective therapeutic approach.

1.5. Santalum album and Its Phytochemicals

Santalum album, commonly known as sandalwood, is a valuable plant species renowned for its fragrant heartwood, essential oil, and pharmacological properties [33]. Various phytochemicals derived from *S. album* have been reported to possess anticancer activity against various cancer cell lines, including melanoma [36], breast cancer [37], and prostate cancer [38]. One of the major components of sandalwood oil, α-santalol, has been shown to induce apoptosis, inhibit cell proliferation, and suppress metastasis through various mechanisms, such as modulating signaling pathways, inducing oxidative stress, and disrupting the cell cycle [39]. Additionally, studies on immortalized human keratinocytes (HaCat cells) have demonstrated that Indian sandalwood oil induces autophagic cell death, prevents UV-induced apoptosis, and inhibits cellular proliferation in skin cancer cells [40-42]. Phytochemicals from *S. album* exhibit selective cytotoxicity toward cancer cells while exhibiting minimal toxicity toward normal cells, making them promising candidates for further investigation as potential AQP3 inhibitors [43].

1.6. Research Objectives

In this in-silico research study, we aimed to use molecular docking, molecular dynamics (MD) simulations, ADME/T predictions, and biological activity prediction using various computational tools to investigate the potential of phytochemicals derived from *S. album* as inhibitors of AQP3. By identifying potent and selective AQP3 inhibitors from natural plant sources, this research could contribute to developing novel therapeutic strategies for skin cancer, with the potential for lower toxicity and improved treatment outcomes.

2. Materials and Methods

2.1. Prediction of Plant Species

The DISPEL (Diseases Plants Eliminate) online platform [44] was utilized to identify suitable plant species for evaluating their phytochemicals against the target protein, aquaporin-3 (AQP3). DISPEL is a comprehensive database containing over 60,000 connections between medicinal plants and diseases, encompassing approximately 5,500 plants and 1,000 diseases globally. It is a valuable resource for addressing infectious and non-infectious human diseases. The platform enables users to search for specific plant diseases or perform comparative analyses involving multiple plants and diseases. Interactive visualizations, such as network graphs, facilitate the interpretation of connections between medicinal plants and diseases. In this study, a search for "skin cancer" was conducted, and the *Santalum album* (Indian sandalwood) was identified as a potential therapeutic plant for skin cancer (**Figure 1**).

2.2. Evaluation of Phytochemicals Present in Santalum album

The phytochemicals present in *S. album* were analyzed using the Indian Medicinal Plants, Phytochemistry and Therapeutics 2.0 (IMPPAT 2.0) server [45].

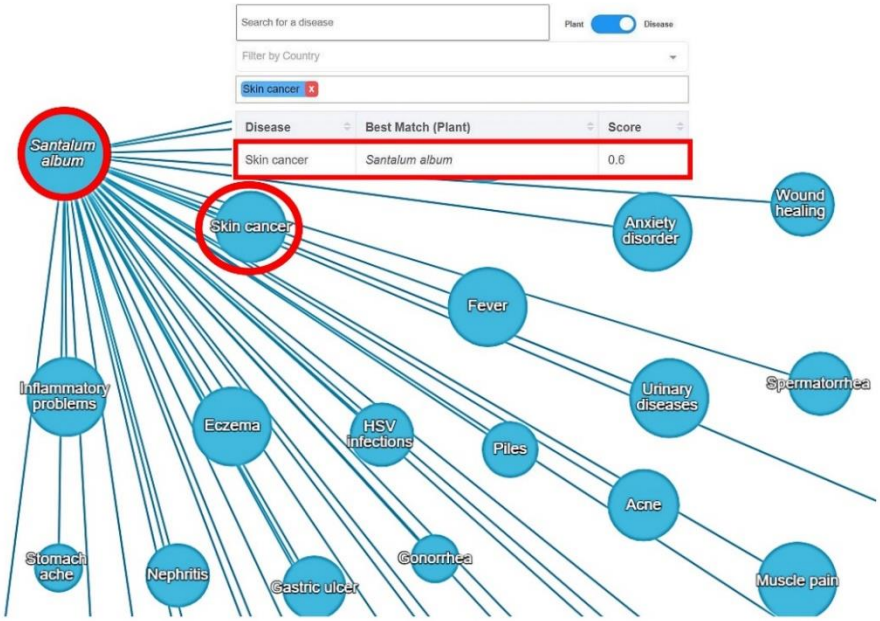

Figure 1. Suitable plant species with therapeutic effects on skin cancer.

IMPPAT 2.0 is an extensive database curated systematically by digitizing data from more than 100 traditional Indian medicine texts, over 7,000 published research articles, and other credible sources. Compared to its predecessor, IMPPAT 1.0, this version offers significant enhancements and expansions, representing the most comprehensive compilation of phytochemical information from Indian medicinal plants. The sdf files of the selected phytochemicals were obtained from the PubChem database.

2.3. Protein Modeling and Structure Validation

The AQP3 protein sequence was retrieved from the UniProt database (accession ID: Q92482) with a high annotation score of 5 out of 5, indicating strong experimental validation through methods such as Edman sequencing, mass spectrometry, X-ray or NMR structure determination, protein-protein interactions, and antibody detection. Homology modeling of the AQP3 3D structure was performed using the SWISS-MODEL server [46], which employs the ProMod3 [47] comparative modeling engine based on OpenStructure. The modeling process involved extracting initial structural information from template structures, addressing insertions and deletions through sequence alignment, and selecting final candidates using statistical scoring methods based on mean force potentials. Non-conserved side chains were modeled using an in-house rotamer library and optimized using the TreePack algorithm [48] and SCWRL4 energy function [49]. Energy minimization was performed using the OpenMM library [50] and the CHARMM22/CMAP force field [51].

The quality and reliability of the AQP3 model were evaluated using multiple analytical techniques, including Ramachandran plot analysis, MolProbity [52] for stereochemical quality assessment, Global Model Quality

Estimate (GMQE) [53], MolProbity score, and QMEAN Z-score. Specific parameters and settings used in these analyses are provided in the Supplementary Information.

2.4. Ligand Retrieval and Preparation

The selected phytochemicals were retrieved from the PubChem database using the sdf file format. PubChem is a comprehensive repository for chemical compounds and their interactions with biological assays, maintained by the National Center for Biotechnology Information (NCBI), a division of the National Library of Medicine (NLM) under the United States National Institutes of Health (NIH). The ligands were prepared using UCSF Chimera version 1.15 [54], a versatile molecular structure visualization and analysis software. Structure optimization was performed using the steepest descent and conjugate gradient energy minimization methods within UCSF Chimera. The ligands selected for virtual screening and their respective PubChem IDs and molecular weights (MWs) are listed in **Table 1**.

2.5. Virtual Screening of Phytochemicals

Virtual screening of the selected phytochemicals was carried out using AutoDock Vina 1.2.0 [55], integrated into PyRx 0.8 [56], a computational tool commonly employed in drug discovery for virtual screening of compound libraries against potential drug targets. AutoDock Vina is a widely used open-source docking software known for its efficiency and scoring mechanism. The specific docking parameters and settings used in this study are detailed in the Supplementary Information.

Table 1. Chosen phytochemicals with their molecular weights (MWs) and PubChem IDs**.**

Ligands	PubChem IDs	Molecular weights (MWs)
Ximenynic acid	5312688	278.4
1-Triacontanol	68972	438.8
Palmitic acid	985	256.42
Betulinic acid	64971	456.7
gamma-Curcumene	12304273	204.35
Alpha-Bergamotenol	5368743	220.35
Beta-Santalene	10889018	204.35
Levomenol	442343	222.37
6-Epi-beta-bisabolol	12300148	222.37
Acoradiene	90351	204.35
trans-alpha-ergamotene	6429302	204.35
Campherene-2,13-diol	42608198	238.37
Himachalol	121536	222.37
germacrene C	25244915	204.35
Sclareol	163263	308.5
Cuparene	86895	202.33
Beta-Oplopenone	14038847	220.35
Lupeol	259846	426.7
Norecasantalic acid	100966488	180.24
Nuciferol	6430906	218.33

2.6. Visualization of Docking Results

The visualization and analysis of the best-docked poses of the hit compounds were conducted using Discovery Studio 4.5 [57]. This software facilitated the exploration of the binding modes and ligand-receptor interactions through 2D and 3D representations.

2.7. Drug-likeness and Physicochemical Property Prediction

The SWISS ADME web server [58] was employed to evaluate the physicochemical properties and drug-likeness of the compounds. This tool computes various descriptors, such as topological polar surface area (TPSA), xlogp3 (lipophilicity), logS (solubility), the number of hydrogen acceptors and donors, and molecular

weight. Additionally, it identifies instances where compounds violate Lipinski's Rule of Five [59], which outlines essential criteria for orally active drugs to demonstrate pharmacological efficacy. The specific parameters and thresholds used for drug-likeness assessment are provided in the Supplementary Information.

2.8. Prediction of Biological Activity

The PASS web server (http://www.pharmaexpert.ru/passonline) [60] was used to predict the biological activities of the selected molecules. PASS Online leverages detailed atom neighbor descriptors to forecast diverse biological activities, encompassing pharmacological effects, mechanisms of action, toxic and adverse effects, interactions with metabolic enzymes and transporters, and impacts on gene expression, among others. The specific activity prediction criteria and thresholds used in this study are detailed in the Supplementary Information.

2.9. ADME/T Analysis

The ADMETlab 2.0 web server [61] was employed for the compounds' Absorption, Distribution, Metabolism, Excretion, and Toxicity (ADME/T) analysis. ADMETlab 2.0 offers a significant expansion in supported ADME/T-related endpoints compared to its previous version, nearly doubling the number of endpoints covered. This includes predictions for 17 physicochemical properties, 13 medicinal chemical properties, 23 ADME properties, 27 toxicity endpoints, and eight toxicophore rules comprising 751 substructures. The specific ADME/T parameters and prediction models used in this study are provided in the Supplementary Information.

2.10. Molecular dynamic simulation

Molecular dynamics (MD) simulations were performed on the modeled AQP3 structure in a complex with selected phytochemicals. These simulations were carried out using the WEBGRO Macromolecular Simulations server (https://simlab.uams.edu/ProteinWithLigand/protein_with_ligand.html) provided by the University of Arkansas for Medical Sciences (UAMS) through the GRACE High-Performance Computing Facility. Prior to the MD simulations, molecular topologies for the specified compounds were generated using the GlycoBioChemPRODRG2 server (http://davapc1.bioch.dundee.ac.uk/cgi-bin/prodrg). The GROMOS96 43A1 force field was employed for MD simulations of AQP3 with the identified compounds, utilizing the SPC water model within a triclinic system and sodium chloride. Energy minimization of the formed complexes was conducted using a steepest descent integrator, followed by equilibration under NVT/NPT conditions at 300 K and 1 bar pressure. The MD simulations were performed with a Leap-Frog integrator, spanning a simulation time of 50 ns (subject to available computational resources) with a fixed frame count of 1000 frames. The parameters and settings used for energy minimization, equilibration, and MD simulations are detailed in the Supplementary Information. The trajectories obtained from the MD simulations were analyzed to evaluate the following parameters: root-mean-square deviation

(RMSD), root-mean-square fluctuation (RMSF), radius of gyration (Rg), and solvent-accessible surface area (SASA) at 300 K. These analyses provide insights into the dynamics and stability of the AQP3-phytochemical complexes. The results from the various computational analyses were interpreted and integrated to conclude the potential of the selected phytochemicals as inhibitors or modulators of AQP3. Specifically, the docking results were evaluated based on the binding affinities and interactions between the phytochemicals and the AQP3 protein structure. The drug-likeness and ADME/T predictions were used to assess the pharmacokinetic and pharmacodynamic properties of the compounds, as well as their potential for further development as drug candidates. The MD simulations provided valuable insights into the dynamic behavior and stability of the AQP3-phytochemical complexes over time. The RMSD, RMSF, Rg, and SASA analyses were used to assess the complexes' conformational changes, flexibility, compactness, and solvent exposure [62-64]. These analyses aided in identifying the most promising phytochemicals with favorable binding interactions and stability profiles. The interpretation of the computational results was further supported by comparative analyses with existing literature and experimental data, where available. Limitations and potential sources of error in the computational approaches were also acknowledged and discussed.

3. Results and Discussion

3.1. Structure prediction, modeling, and validation of target protein

The AQP3 sequence obtained from UniProt (accession ID: Q92482) was the reference sequence for modeling AQP3 using the SWISSMODEL server.

BLAST was employed to identify a suitable template sequence, leading to the selection of the crystal structure of human AQP10 as the template sequence (with a 50.76% identity) for modeling AQP3. The 3D structure of the modeled AQP3 is depicted in **Figure 2**.

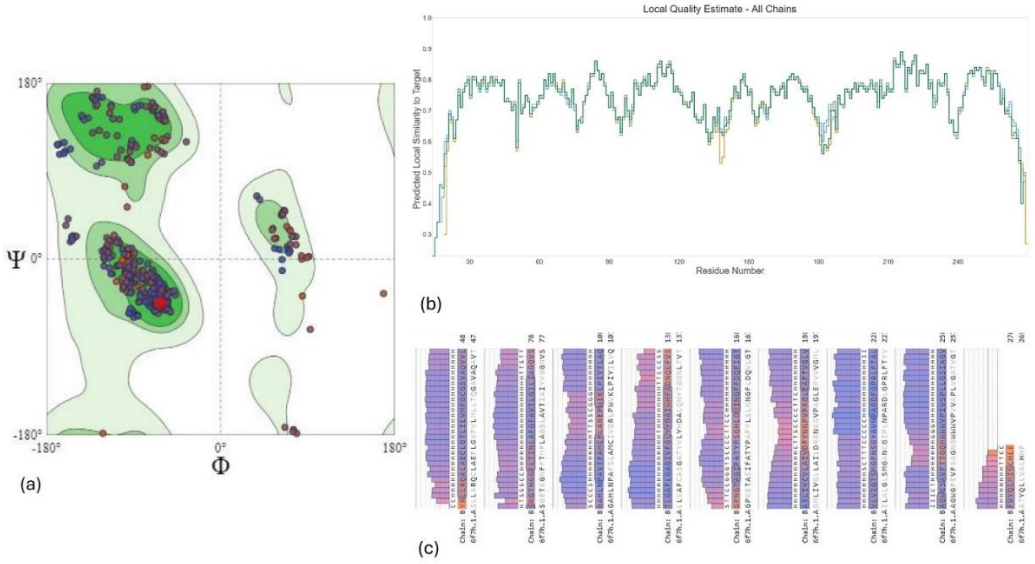

Figure 2. Depiction of the Ramachandran plot (a), local quality estimate (b), and sequence alignment (c) of the modeled structure. It was observed that 95.12% of the residues lie in the favored region.

Furthermore, the modeled structure was validated based on various scores to evaluate its quality and reliability. The GMQE (Global Model Quality Estimation) score, ranging from 0 to 1, indicates the model's overall quality. A higher GMQE closer to 1 indicates a more satisfactory structure. In this instance, the GMQE for the modeled structure was 0.70, suggesting relatively good quality. The MolProbity score, with an observed value of 1.61, is another critical metric for assessing model quality. A MolProbity score greater than -4 and less than two is appropriate for the modeled structure, providing insights into steric clashes and overall geometry.

Additionally, the QMEAN Z-score was used to evaluate the global and local quality of the modeled structure, where a score below -4 indicates low quality.

In this case, the QMEAN Z-score was -3.29, suggesting acceptable quality. Furthermore, Ramachandran analysis was conducted to assess the backbone conformation, revealing that 95.12% of the residues were within the favored region of the Ramachandran plot, indicating good stereochemical quality. **Figure 2** shows the Ramachandran plot and local quality estimate, which provides visual insights into the quality of the modeled AQP3 structure. These validation metrics collectively enhance confidence in the reliability and utility of the modeled AQP3 structure for further studies and analyses.

3.2. Virtual screening of phytochemicals

The docking study utilized the modeled 3D crystal structure of AQP3, with AutoDock Vina accessed through PyRx 0.8 serving as the analysis tool. The Dockprep feature of UCSF Chimaera was utilized to prepare the protein for docking. The protein transformed a macromolecule, and the selected compounds underwent initial minimization using the mmff94 force field while polar hydrogens were added. Subsequently, the compounds were converted to pdbqt format using Open Babel within PyRx. For the blind docking procedure, a grid box with dimensions of 67.48 Å × 80.90 Å × 76.14 Å was employed, centered at the following coordinates (77.71, -64.68, and 64.65). The exhaustiveness level was set to the default value of 8. Specific details regarding the ligands or compounds and their respective docking scores (kcal/mol) are provided in **Figure 3**. Docking scores reflect the binding affinity of a ligand toward its target protein, offering insights into the potential effectiveness of the ligand as a therapeutic agent. Lower docking scores typically signify stronger binding affinity and greater potential for drug efficacy. Phytochemicals with docking scores of -7 or less were selected for further analysis.

3.3. Evaluation of physiochemical properties and drug-likeness

The SWISS ADME webserver was utilized to analyze the physicochemical properties of the sorted phytochemicals from previous steps (**Table 2**). Various parameters, including solubility (LogS), skin permeation (Log Kp), hydrogen bond acceptors (Accept H), hydrogen bond donors (Donor H), topological polar surface area (TPSA), and gastrointestinal (GI) absorption, were assessed. The drug-likeness properties of the phytochemicals were evaluated based on Lipinski's rule of five, where adherence to the rule suggests favorable drug-like properties.

Acoradiene exhibits a relatively high LogS value, indicating good aqueous solubility. However, it is predicted to have low GI absorption, suggesting limited oral bioavailability due to its lack of hydrogen bond acceptors and donors. Alpha-bergamotenol demonstrated moderate LogS value and high Log Kp, indicating good solubility and permeability with favorable GI absorption potential. Beta-santalene displays good solubility but limited permeability and is predicted to have low GI absorption, similar to Cuparene, Germacrene C, and Trans-alpha-Bergamotene. With multiple hydrogen bond acceptors and donors, betulinic acid shows excellent solubility but poor permeability, suggesting potential interactions with biological targets but low GI absorption.

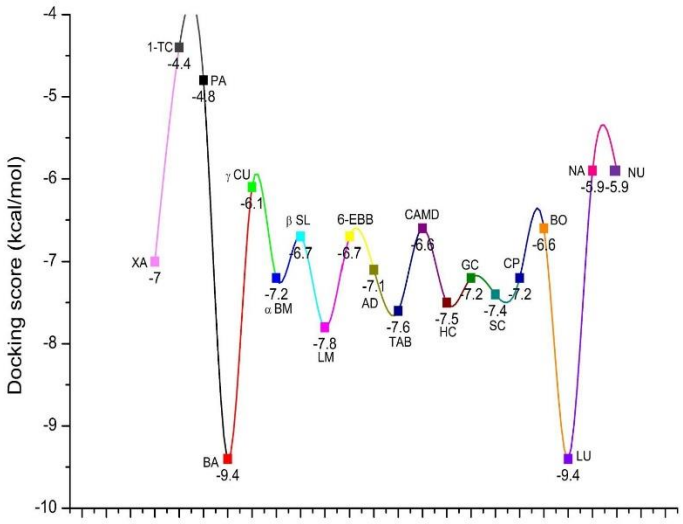

Ligands	Docking scores (kcal/mol)
Ximenynic acid (XA)	-7.0
1-Triacontanol (1-TC)	-4.4
Palmitic acid (PA)	-4.8
Betulinic acid (BA)	-9.4
Gamma-Curcumene (γ CU)	-6.1
Alpha-Bergamotenol (α BM)	-7.2
Beta-Santalene (β SL)	-6.7
Levomenol (LM)	-7.8
6-Epi-beta-bisabolol (6-EBB)	-6.7
Acoradiene (AD)	-7.1
trans-alpha-Bergamotene (TAB)	-7.6
Campherene-2,13-diol (CAMD)	-6.6
Himachalol (HC)	-7.5
Germacrene C (GC)	-7.2
Sclareol (SC)	-7.4
Cuparene (CP)	-7.2
Beta-Oplopenone (BO)	-6.6
Lupeol (LU)	-9.4
Norecasantalic acid (NA)	-5.9
Nuciferol (NU)	-5.9

Figure 3. Docking score (kcal/mol) of the chosen phytochemicals.

Table 2. Physiochemical properties and drug-likeness properties of phytochemicals according to the SWISS ADME server**.**

Ligands	LogS	Log K_p	Accept H	Donor H	TPSA (Å)	GI absorption	Drug-likeness
Acoradiene	5.12	-3.91	0	0	0	Low	Yes
Alpha-Bergamotenol	-4.22	-3.95	1	1	20.23	High	Yes
Beta-Santalene	-4.81	-3.15	0	0	0	Low	Yes
Betulinic acid	-7.71	-3.26	3	2	57.53	Low	Yes
Cuparene	-4.77	-3.65	0	0	0	Low	Yes
Germacrene C	-4.54	-3.61	0	0	0	Low	Yes
Himachalol	-3.42	-5.18	1	1	20.23	High	Yes
Lupeol	-8.64	-1.90	1	1	20.23	High	Yes
Levomenol	-3.34	-4.97	1	1	20.23	High	Yes
Sclareol	-4.59	-4.46	2	2	40.46	High	Yes
Ximenynic acid	-5.17	-3.05	2	1	37.30	High	Yes
Trans-alpha-Bergamotene	-4.97	-2.97	0	0	0	Low	Yes

Phytochemicals such as alpha-bergamotenol, Himachalol, Lupeol, Levomenol, Sclareol, and Ximenynic Acid exhibit good solubility and permeability, along with high GI absorption potential, making them suitable candidates for oral administration. Based on their GI absorption properties, phytochemicals with low GI absorption were excluded from further analysis, while those with high GI absorption were selected for further investigation.

3.4. Biological activity prediction of phytochemicals

PASS webserver was used to predict the biological activity of the identified phytochemicals. "Dermatologic" and "antineoplastic" activity was considered (**Table 3**). The probability of being active (Pa) for dermatologic properties ranged between 0.473 and 0.736, while the probability of being inactive (Pi) ranged between 0.006 and 0.038.

For antineoplastic properties, the value of Pa ranged between 0 and 0.950. A Pa value that surpasses the Pi value indicates the probable presence of the specified biological activity. The summarized outcomes are presented in **Table 3**. Lupeol demonstrates exceptionally high probabilities of dermatologic and antineoplastic activities, indicating its potential as a multifunctional therapeutic agent.

Similarly, Himachalol, Sclareol, and Levomenol exhibit significant probabilities of dermatologic and antineoplastic activities, suggesting their promising roles in dermatological and anticancer applications. Alpha-bergamotenol presents moderate probabilities of dermatologic and antineoplastic activities, indicating its potential utility in skin-related disorders and cancer treatment. Ximenynic acid was excluded from subsequent analysis due to its absence of predicted antineoplastic activity, as indicated by predictions of the PASS server.

Table 3. Biological activity prediction of compounds (Pa= probability of being active; Pi= probability of being inactive)**.**

Ligands	Biological activity	Pa	Pi
Alpha-Bergamotenol	Dermatologic	0.57	0.02
	Antineoplastic	0.51	0.06
Himachalol	Dermatologic	0.59	0.01
	Antineoplastic	0.65	0.03
Levomenol	Dermatologic	0.65	0.01
	Antineoplastic	0.65	0.03
Lupeol	Dermatologic	0.73	0.006
	Antineoplastic	0.95	0.004
Sclareol	Dermatologic	0.60	0.01
	Antineoplastic	0.64	0.03
Ximenynic acid	Dermatologic	0.47	0.03
	Antineoplastic	---	---

3.5. ADME/T analysis

The ADMET Lab 2.0 server was used to analyze their ADME/T properties. The various properties considered and their respective observed values are given in **Table 4**. The optimal range for different values is defined in the Table legend. The moderate permeability of alpha-Bergamotenol across Caco-2 cells signifies its potential for intestinal absorption, which is a pivotal factor in drug bioavailability. Notably, its neutrality as both a substrate and inhibitor of P-glycoprotein suggests an absence of active efflux or transport inhibition. This characteristic, coupled with its moderate tissue distribution and negligible metabolism by the key CYP enzyme CYP2D6, indicates favorable pharmacokinetic properties.

Furthermore, its high clearance rate and absence of observed toxicity across various endpoints, including carcinogenicity, hepatotoxicity, AMES toxicity, and respiratory toxicity, underscore its potential safety profile. Himachalol, which exhibits comparable permeability across Caco-2 cells, also has the potential for intestinal absorption potential. Its neutral interaction with P-glycoprotein and moderate tissue distribution reinforces this likelihood. Although it was identified as a substrate for CYP2D6 and CYP2C9, its potential metabolism, moderate clearance rate, and lack of toxicity across various endpoints suggest favorable pharmacokinetic characteristics. However, the observed respiratory toxicity warrants careful consideration, prompting its exclusion from further analysis due to potential safety concerns in this context. Sclareol, like its counterparts, shows moderate permeability across Caco-2 cells, suggesting plausible intestinal absorption.

The lack of discernible interactions with P-glycoprotein, relatively high tissue distribution, and identification as a substrate for CYP2C9 suggest potential metabolic pathways. However, its high clearance rate and absence of toxicity across various endpoints support its pharmacokinetic suitability for further evaluation. Lupeol has rapid elimination kinetics and is distinguished by its minimal metabolism by the key CYP enzymes CYP2D6 and CYP3A4 and its high clearance rate.

Moreover, its nontoxic profile across evaluated endpoints bolsters its pharmacokinetic feasibility for consideration in drug development endeavors. Levomenol, characterized by relatively low tissue distribution and identification as a substrate for CYP2C9, suggests potential metabolic pathways. Like Lupeol's, its high clearance rate signifies efficient elimination kinetics. Furthermore, its nontoxicity profile across various endpoints supports its pharmacokinetic suitability for further exploration.

Table 4. ADME/T analysis of selected phytochemicals as predicted by ADMET LAB 2.0. Optimal value: Caco-2 permeability; >5.15 log unit, volume distribution; 0.04 to 20 L/kg, clearance; (high= >15 mL/min/kg: moderate= 5-15 mL/min/kg: low= <5 mL/min/kg).

Parameters	Alpha-ergamotenol	Himachalol	Sclareol	Lupeol	Levomenol
Caco-2 Permeability	-4.344	-4.485	-4.627	-5.020	-4.387
P-glycoprotein substrate	Negative	Negative	Negative	Negative	Negative
P-glycoprotein inhibitor	Negative	Negative	Negative	Negative	Negative
Distribution					
Volume distribution	3.141	2.43	3.16	1.73	3.37
Metabolism					
CYP2C9 substrate	Non-substrate	Substrate	Substrate	Non-substrate	Substrate
CYP2D6 substrate	Substrate	Substrate	Non-substrate	Substrate	Non-substrate
CYP3A4 substrate	Non-substrate	Non-substrate	Non-substrate	Substrate	Non-substrate
CYP1A2 inhibition	Non-inhibitor	Non-inhibitor	Non-inhibitor	Non-inhibitor	Non-inhibitor
CYP2C9 inhibition	Non-inhibitor	Non-inhibitor	Non-inhibitor	Non-inhibitor	Non-inhibitor
CYP2D6 inhibition	Non-inhibitor	Non-inhibitor	Non-inhibitor	Non-inhibitor	Non-inhibitor
CYP2C19 inhibition	Non-inhibitor	Non-inhibitor	Non-inhibitor	Non-inhibitor	Non-inhibitor
Excretion					
Clearance	17.33	9.81	17.66	17.92	17.91
Toxicity					
Carcinogenicity	Inactive	Inactive	Inactive	Inactive	Inactive
Hepatotoxicity	Inactive	Inactive	Inactive	Inactive	Inactive
AMES Toxicity	Inactive	Inactive	Inactive	Inactive	Inactive
Respiratory toxicity	Inactive	Active	Inactive	Inactive	Inactive

3.6. Molecular dynamic simulation

Through meticulous exploration of receptor-inhibitor complexes using MD analysis, this study aimed to determine RMSF, RMSD, SASA, and Rg parameters. These simulations contribute significantly to understanding the strength of interactions between these molecules, aiding in predicting the stability of the receptor-ligand complex.

The RMSD trajectories derived from the MD simulations validated the data acquired from the docking studies (**Figure 4**). Among the selected phytochemicals, sclareol demonstrated the lowest RMSD fluctuation, indicating higher stability of the AQP3-sclareol complex than the complexes formed with other ligands. Lupeol exhibited high fluctuation around 25 ns but stabilized after that, while alpha-bergamotenol showed significant fluctuation around 43 ns, suggesting relatively lower stability of these complexes.

Analysis of the radius of gyration (Rg) revealed that sclareol maintained maximum compactness of the AQP3 structure, as evidenced by its minimal Rg values (**Figure 5**). In contrast, levomenol and lupeol exhibited significant fluctuations in compactness, implying reduced stability of their respective complexes with AQP3.

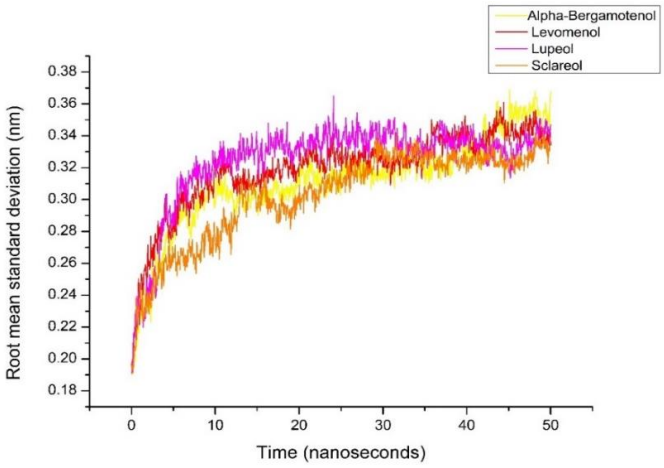

Figure 4. Root mean square deviation of receptor-ligand complex: alpha-bergamotenol (yellow), levomenol (red), lupeol (magenta), and sclareol (golden).

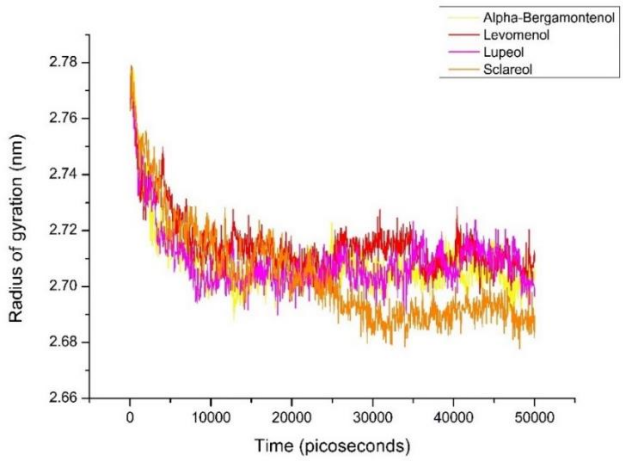

Figure 5. The radius of gyration (Rg) of the receptor-ligand complex: alpha-bergamot enol (yellow), levomenol (red), lupeol (magenta), and sclareol (golden).

The RMSF analysis (**Figure 6**) indicated that sclareol exhibited the least fluctuation compared to other ligands, suggesting its potential as a more effective inhibitor of AQP3. Among the selected ligands, sclareol displayed the lowest SASA values, further reinforcing the compactness and stability of the AQP3-sclareol complex (**Figure 7**).

These analyses suggest that sclareol forms the most stable complex with AQP3 among the selected phytochemicals, potentially making it the most promising candidate for further evaluation as an AQP3 inhibitor.

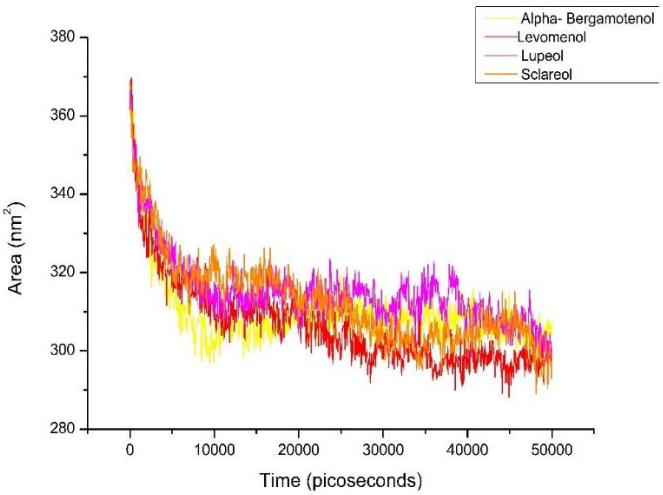

Figure 7. Solvent-accessible surface area (SASA) evaluation of various receptor-ligand complexes: alpha-bergamot enol (yellow), levomenol (red), lupeol (magenta), and sclareol (golden).

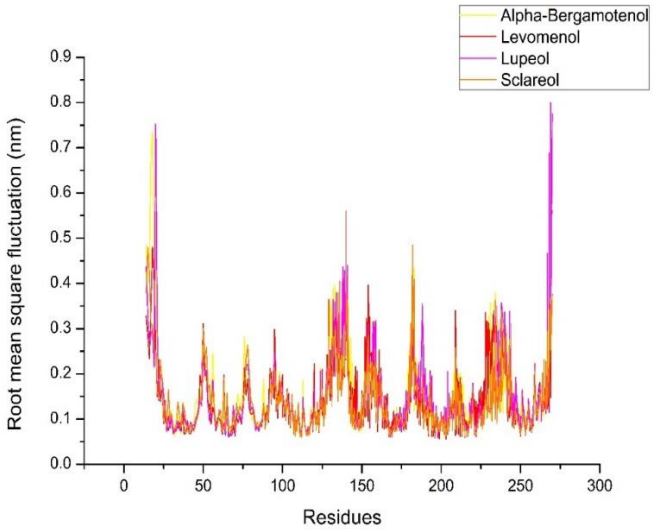

Figure 6. Root mean square fluctuation (RMSF) of the receptor-ligand complex: alpha-bergamot enol (yellow), levomenol (red), lupeol (magenta), and sclareol (golden).

3.7. Visualization and interaction of the best-docked poses

A schematic representation of the best-docked pose and interaction of each of the hit compounds (**Table 5**), namely, alpha-bergamotenol, levomenol, lupeol, and sclareol with AQP3 is depicted in **Figure 8 (a-d)**.

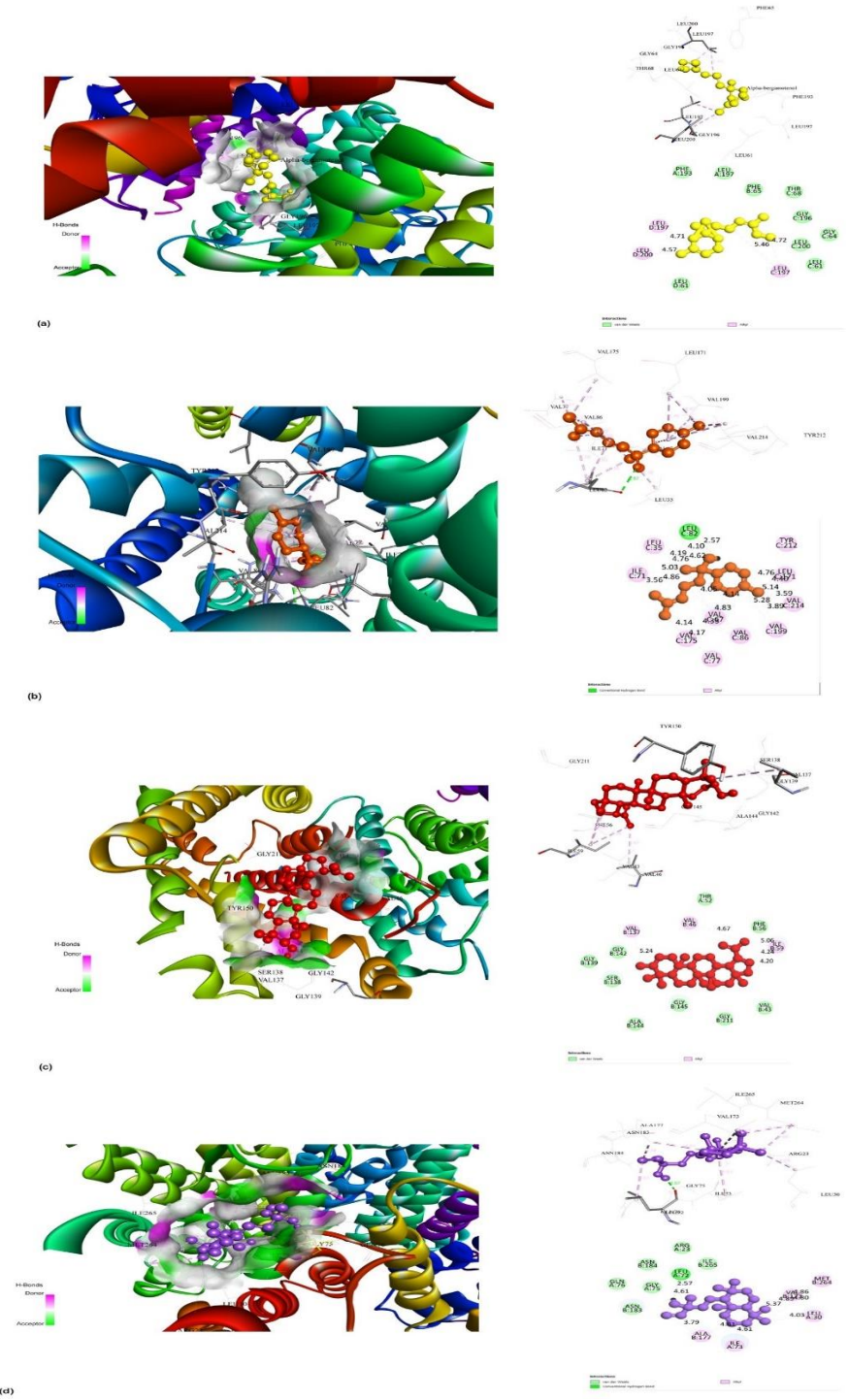

Figure 8. Schematic representation of best-docked poses and interaction of the ligands with the active site of the target protein: (a) alpha-bergamotenol (b) levomenol (c) lupeol (d) sclareol.

Table 5. The chosen phytochemicals (ligands) interact with the active site of the target protein AQP3, demonstrating various types of interactions such as van der Waals, alkyl, and hydrogen bonding interactions. The table details the interacting residues and the type of interaction observed**.**

Ligands	Interactions	Amino acids	Bond length (Å)
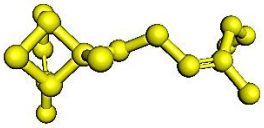 **Alpha-bergamotenol**	van der Waals	Phe193A, Phe197A, Phe65B, Leu61C, Gly64C, Thr68C, Gly196C, Leu200C, Leu61D	----
	Alkyl	Leu197C	4.73, 5.46
		Leu197D	4.71
		Leu200D	4.57
Levomenol 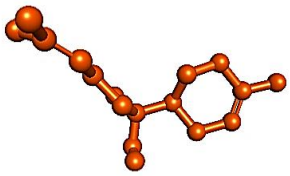	Alkyl	Leu35C	4.78
		Val67C	4.10, 4.32
		Ile71C	3.76, 5.13, 6.04
		Val77C	4.06
		Leu82C	4.26, 4.56, 4.99
		Val88C	5.05, 5.69
		Leu171C	5.04, 6.61
		Val175C	4.74
		Val199C	4.20, 6.91
		Val214C	4.15,6.63
	Hydrogen bonding	Leu82C	2.57
Lupeol 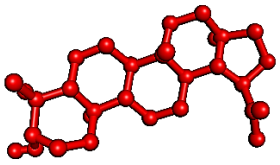	van der Waals	Thr52A, Phe56B, Thr52B, Ser138B, Gly139B, Val143B, Ala144B, Gly145B, Gly211B	----
	Alkyl	Val46B	**4.67**
		Ile59B	**4.20, 4.24, 5.06**
		Val137B	**5.24**
Sclareol 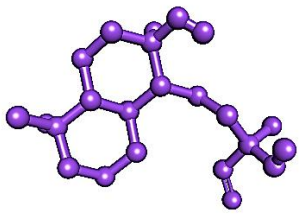	van der Waals	Arg73A, Gly75, Gln76A, Asn183B, Asn184B, Ile265B	----
	Alkyl	Leu30A	4.03
		Leu72A	4.61
		Ile73A	4.61
		Val173B	4.89, 5.37
		Ala177B	3.79, 4.81
		Met264B	4.80, 4.86
	Hydrogen bonding	Leu72A	2.57

Alpha-bergamotenol interacts with aromatic residues such as phenylalanine (Phe) and hydrophobic residues such as leucine (Leu) through van der Waals interactions. The absence of the bond length suggests that interactions are more based on proximity and shape complementarity than direct bonding. It forms alkyl interactions with Leu197C, Leu197D, and Leu200D, with bond lengths ranging from 4.57 to 5.46 Å. These interactions involve hydrophobic contacts between the ligand's alkyl groups and the hydrophobic side chains of the amino acids. Levomenol primarily engages in alkyl interactions with various residues such as Leu, valine (Val), and isoleucine (Ile) at different positions.

Additionally, there is a hydrogen bonding interaction with Leu82C, which has a bond length of 4.49 Å. Alkyl interactions facilitate hydrophobic interactions, while hydrogen bonding increases the specificity and stability of the ligand-protein complex. Lupeol interacts via van der Waals forces with residues such as threonine (Thr), Phe, and glycine (Gly). It also forms alkyl interactions with varying bond lengths with Val46B, Ile59B, and Val137B. Sclareol interacts through van der Waals forces with residues such as arginine (Arg), Gly, and glutamine (Gln). It forms alkyl interactions with Leu, Ile, Val, Ala, and Met residues with varying bond lengths. Sclareol also participates in a hydrogen bonding interaction with Leu72A, with a bond length of 2.57 Å. Among the amino acids identified in the interactions, Leu is the most abundant in the binding pocket of AQP3. This high frequency suggests Leu residues play a significant role in mediating ligand binding, likely due to their hydrophobic nature and involvement in alkyl interactions with the ligands. In addition to leucine, valine is the second most abundant amino acid, reinforcing its importance in contributing to the hydrophobic interactions that stabilize protein-ligand complexes.

Considering the presence of hydrogen bonding and the number of interactions, compared with the other ligands listed in the table, sclareol and levomenol appear to have the potential to form a more stable complex with the protein. The hydrogen bonding interaction, in addition to van der Waals and alkyl interactions, contributes to the specificity and strength of the ligand-protein complex, potentially leading to increased stability.

3.8. Limitations and future directions

While the computational approaches employed in this study provide valuable insights into the potential of the selected phytochemicals as AQP3 inhibitors, it is important to acknowledge certain limitations. Firstly, the accuracy of the molecular dynamics simulations and subsequent analyses depends on the accuracy of the initial homology model of AQP3.

Furthermore, the computational predictions and assessments may not fully capture the complex biological environment and interactions in living systems.

Future research directions could involve experimental validation of the computational findings, including in vitro and in vivo studies, to assess the efficacy and safety of the identified phytochemicals as AQP3 inhibitors. Additionally, the most promising candidates' structural optimization and chemical modifications could be explored to enhance their potency and pharmacokinetic properties further. Lastly, investigating the potential synergistic effects of these phytochemicals in combination with other therapeutic agents may provide opportunities for more effective treatment strategies.

The present study employed a comprehensive computational approach to identify potential aquaporin-3 (AQP3) protein inhibitors derived from phytochemicals found in the *Santalum album*. This investigation is relevant in developing novel therapeutic strategies for melanoma and other skin cancers, as AQP3 has been implicated in tumor growth, angiogenesis, and metastasis. The initial step involved homology modeling of the AQP3 structure, which yielded a satisfactory model

with acceptable quality scores, including the GMQE, MolProbity, and QMEAN Z-scores. The subsequent virtual screening of phytochemicals using AutoDock Vina enabled the identification of compounds with binding solid affinities for AQP3, focusing on those exhibiting docking scores of -7 or lower. This approach leveraged the strength of computational docking simulations to prioritize potential hit compounds for further evaluation.

Evaluation of the physicochemical properties and drug-likeness using SWISS ADME provided insights into the selected compounds' solubility, permeability, and gastrointestinal absorption. Adherence to Lipinski's Rule of Five facilitated the identification of compounds suitable for oral administration, a critical consideration for drug development. The biological activity prediction using the PASS webserver revealed the potential dermatologic and antineoplastic activities of phytochemicals such as alpha-bergamotenol, lupeol, himachalol, sclareol, and levomenol, highlighting their multifunctional therapeutic potential.

The ADME/T analysis using the ADMET Lab 2.0 server offered valuable information regarding the compounds' pharmacokinetic properties and safety profiles. Compounds like alpha-bergamotenol, sclareol, levomenol, and lupeol demonstrated favorable properties, including intestinal absorption potential and no observed toxicity, while himachalol exhibited respiratory toxicity, prompting its exclusion from further consideration.

MD simulations provided insights into the dynamic behavior and stability of the receptor-ligand complexes over time. Analyses of RMSD, Rg, RMSF, and SASA revealed that compounds such as sclareol and levomenol exhibited stable interactions with AQP3, reinforcing their potential as potent inhibitors. The visualization and interaction analysis of the best-docked poses further elucidated the binding mechanisms, highlighting the presence of hydrogen bonding interactions and alkyl interactions with key residues, contributing to the stability of the receptor-ligand complexes.

It is important to note that while computational approaches provide valuable insights and prioritize potential hit compounds, experimental validation is crucial to confirm the efficacy and safety of these compounds as AQP3 inhibitors. Future research directions could involve in vitro and in vivo studies to evaluate the identified phytochemicals' biological activities and pharmacokinetic properties. Additionally, the most promising candidates' structural optimization and chemical modifications may further enhance their potency and pharmacokinetic characteristics.

Furthermore, exploring the potential synergistic effects of these phytochemicals in combination with other therapeutic agents could pave the way for more effective treatment strategies. It is also essential to consider the identified compounds' potential off-target effects and toxicity profiles, as these factors can significantly influence their clinical applicability and safety profiles.

4. Conclusion

A comprehensive molecular docking study of phytochemicals derived from *S. album* that inhibit AQP3 yielded promising results, as detailed through various computational

analyses. This research integrated structural modeling, virtual screening, physicochemical property evaluation, biological activity prediction, ADME/T analysis, molecular dynamic simulations, and interaction analysis to identify potential therapeutic candidates. The structural modeling of AQP3 using SWISSMODEL, coupled with validation metrics such as the GMQE score, MolProbity score, QMEAN Z-score, and Ramachandran analysis, ensured the reliability and quality of the modeled AQP3 structure. This provided a robust foundation for subsequent molecular docking studies. Virtual screening of phytochemicals involved meticulous protein and compound preparation, followed by blind docking using AutoDock Vina. The assessment of docking scores facilitated the identification of compounds with potential therapeutic efficacy against AQP3, focusing on those exhibiting docking scores of -7 or less. Using SWISS ADME to evaluate physiochemical properties and drug-likeness highlighted compounds with favorable solubility, permeability, and gastrointestinal absorption. Lipinski's rule of five aided in selecting compounds suitable for oral administration. The PASS webserver's Biological activity prediction revealed the potential dermatologic and antineoplastic activities of selected phytochemicals. Compounds such as alpha-bergamotenol, lupeol, himachalol, sclareol, and levomenol exhibited significant probabilities of both activities, suggesting their multifunctional therapeutic potential. Subsequent analysis of ADME/T properties using the ADMET Lab 2.0 server provided insights into the compounds' pharmacokinetic characteristics and safety profiles. Compounds such as alpha-bergamotenol, sclareol, levomenol, and lupeol demonstrated favorable properties, including intestinal absorption potential and no toxicity, while himachalol exhibited respiratory toxicity. Molecular dynamic simulations allowed exploration of the dynamic interactions between the receptor and ligands over time. RMSD, Rg, RMSF, and SASA analyses provided valuable insights into the receptor-ligand complexes' stability, compactness, and flexibility. Compounds such as sclareol and levomenol exhibited stable interactions with AQP3, suggesting their potential as potent inhibitors. Finally, visualization and interaction analysis of the best-docked poses provided a detailed understanding of the binding mechanisms of the phytochemicals with AQP3. Compounds such as sclareol and levomenol displayed hydrogen bonding and alkyl interactions with key residues, indicating their potential for stable complex formation. This comprehensive computational study identified phytochemicals levomenol and sclareol from *S. album* as promising inhibitors of AQP3, with potential therapeutic implications in dermatologic conditions and melanoma treatment. Further experimental validation is warranted to confirm the efficacy and safety of these compounds for clinical application.

Conflict of interest

The authors declare to have no conflict of interest.

Acknowledgement

The authors would like to acknowledge the Department of Biochemistry, JNMC Medical College, for providing the required facilities for the study.

References

[1] H. Sung, J. Ferlay, R.L. Siegel, M. Laversanne, I. Soerjomataram, A. Jemal, F. Bray, Global Cancer Statistics 2020: GLOBOCAN Estimates of Incidence and Mortality Worldwide for 36 Cancers in 185 Countries, CA Cancer J. Clin. 71(3) (2021) 209-249.

[2] NH. Matthews, W.Q. Li, A.A. Qureshi, M.A. Weinstock, E. Cho, Epidemiology of Melanoma, in: W.H. Ward, J.M. Farma (Eds.), Cutaneous Melanoma: Etiology and Therapy, Codon Publications
The Authors., Brisbane (AU), 2017.

[3] J.G. Einspahr, S.P. Stratton, G.T. Bowden, D.S. Alberts, Chemoprevention of human skin cancer, Crit. Rev. Oncol. Hematol. 41(3) (2002) 269-85.

[4] D. Didona, G. Paolino, U. Bottoni, C. Cantisani, Non Melanoma Skin Cancer Pathogenesis Overview, Biomedicines 6(1) (2018).

[5] S. Marlar, H.H. Jensen, F.H. Login, L.N. Nejsum, Aquaporin-3 in Cancer, Int J Mol Sci 18(10) (2017).

[6] D.K. Yadav, S. Kumar, E.H. Choi, S. Chaudhary, M.H. Kim, Computational Modeling on Aquaporin-3 as Skin Cancer Target: A Virtual Screening Study, Front Chem 8 (2020) 250.

[7] M. Hara-Chikuma, A.S. Verkman, Aquaporin-3 facilitates epidermal cell migration and proliferation during wound healing, J. Mol. Med. (Berl.) 86(2) (2008) 221-31.

[8] Y. Sugiyama, Y. Ota, M. Hara, S. Inoue, Osmotic stress up-regulates aquaporin-3 gene expression in cultured human keratinocytes, Biochim Biophys Acta 1522(2) (2001) 82-8.

[9] S.K. Agarwal, A. Gupta, Aquaporins: The renal water channels, Indian J. Nephrol. 18(3) (2008) 95-100.

[10] C. Zhu, Z. Chen, Z. Jiang, Expression, Distribution and Role of Aquaporin Water Channels in Human and Animal Stomach and Intestines, Int J Mol Sci 17(9) (2016).

[11] S.Y. Jung, D.C. Park, S.S. Kim, S.G. Yeo, Expression, Distribution and Role of Aquaporins in Various Rhinologic Conditions, Int J Mol Sci 21(16) (2020).

[12] A.S. Verkman, J. Ruiz-Ederra, M.H. Levin, Functions of aquaporins in the eye, Prog. Retin. Eye Res. 27(4) (2008) 420-33.

[13] 13. WB Bollag, L. Aitkens, J. White, K.A. Hyndman, Aquaporin-3 in the epidermis: more than skin deep, Am. J. Physiol. Cell Physiol. 318(6) (2020) C1144-c1153.

[14] R. Zwiech, A. Bruzda-Zwiech, E. Balcerczak, J. Szczepańska, A. Krygier, B. Małachowska, D. Michałek, D. Szmajda-Krygier, A potential link between AQP3 and SLC14A1 gene expression level and clinical parameters of maintenance hemodialysis patients, BMC Nephrol. 23(1) (2022) 297.

[15] C.S. Moon, D. Moon, S.K. Kang, Aquaporins in Cancer Biology, Front. Oncol. 12 (2022) 782829.

[16] Y.L. Liu, T. Matsuzaki, T. Nakazawa, S. Murata, N. Nakamura, T. Kondo, M. Iwashina, K. Mochizuki, T. Yamane, K. Takata, R. Katoh, Expression of aquaporin 3 (AQP3) in normal and neoplastic lung tissues, Hum. Pathol. 38(1) (2007) 171-8.

[17] Y. Machida, Y. Ueda, M. Shimasaki, K. Sato, M. Sagawa, S. Katsuda, T. Sakuma, Relationship of aquaporin 1, 3, and 5 expression in lung cancer cells to cellular differentiation, invasive growth, and metastasis potential, Hum. Pathol. 42(5) (2011) 669-78.

[18] A. Li, D. Lu, Y. Zhang, J. Li, Y. Fang, F. Li, J. Sun, Critical role of aquaporin-3 in epidermal growth factor-induced migration of colorectal carcinoma cells and its clinical significance, Oncol. Rep. 29(2) (2013) 535-40.

[19] M. Kusayama, K. Wada, M. Nagata, S. Ishimoto, H. Takahashi, M. Yoneda, A. Nakajima, M. Okura, M. Kogo, Y. Kamisaki, Critical role of aquaporin 3 on growth of human esophageal and oral squamous cell carcinoma, Cancer Sci. 102(6) (2011) 1128-36.

[20] X. Guo, T. Sun, M. Yang, Z. Li, Z. Li, Y. Gao, Prognostic value of combined aquaporin 3 and aquaporin 5 overexpression in hepatocellular carcinoma, Biomed Res Int 2013 (2013) 206525.

[21] D. Niu, Y. Bai, Q. Yao, W. Hou, L. Zhou, X. Huang, C. Zhao, Expression and Significance of AQP3 in Cutaneous Lesions, Anal. Cell. Pathol. (Amst.) 2021 (2021) 7866471.

[22] Y.T. Huang, J. Zhou, S. Shi, H.Y. Xu, F. Qu, D. Zhang, Y.D. Chen, J. Yang, H.F. Huang, J.Z. Sheng, Identification of Estrogen Response Element in Aquaporin-3 Gene that Mediates Estrogen-induced

Cell Migration and Invasion in Estrogen Receptor-positive Breast Cancer, Sci. Rep. 5 (2015) 12484.

[23] N. Yang, W. Xiao, X. Song, W. Wang, X. Dong, Recent Advances in Tumor Microenvironment Hydrogen Peroxide-Responsive Materials for Cancer Photodynamic Therapy, Nanomicro Lett 12(1) (2020) 15.

[24] C. Prata, S. Hrelia, D. Fiorentini, Peroxiporins in Cancer, Int J Mol Sci 20(6) (2019).

[25] Q. Wang, B. Lin, H. Wei, X. Wang, X. Nie, Y. Shi, AQP3 Promotes the Invasion and Metastasis in Cervical Cancer by Regulating NOX4-derived H(2)O(2) Activation of Syk/PI3K/Akt Signaling Axis, J. Cancer 15(4) (2024) 1124-1137.

[26] H. Xu, Y. Xu, W. Zhang, L. Shen, L. Yang, Z. Xu, Aquaporin-3 positively regulates matrix metalloproteinases via PI3K/AKT signal pathway in human gastric carcinoma SGC7901 cells, J. Exp. Clin. Cancer Res. 30(1) (2011) 86.

[27] A.S. Verkman, M. Hara-Chikuma, M.C. Papadopoulos, Aquaporins--new players in cancer biology, J. Mol. Med. (Berl.) 86(5) (2008) 523-9.

[28] B. Aikman, A. de Almeida, S.M. Meier-Menches, A. Casini, Aquaporins in cancer development: opportunities for bioinorganic chemistry to contribute novel chemical probes and therapeutic agents, Metallomics 10(5) (2018) 696-712.

[29] A. de Almeida, B.L. Oliveira, J.D.G. Correia, G. Soveral, A. Casini, Emerging protein targets for metal-based pharmaceutical agents: An update, Coord. Chem. Rev. 257(19) (2013) 2689-2704.

[30] CM Niemietz, SD. Tyerman, New potent inhibitors of aquaporins: silver and gold compounds inhibit aquaporins of plant and human origin, FEBS Lett. 531(3) (2002) 443-7.

[31] Martins AP, Marrone A, Ciancetta A, Galán Cobo A, Echevarría M, Moura TF, Re N, Casini A, Soveral G. Targeting aquaporin function: potent inhibition of aquaglyceroporin-3 by a gold-based compound. PLoS One. 2012;7(5):e37435. doi: 10.1371/journal.pone.0037435. Epub 2012 May 18. P.M.I.D.: 22624030; P.M.C.I.D.: PMC3356263.

[32] A. Serna, A. Galán-Cobo, C. Rodrigues, I. Sánchez-Gomar, J.J. Toledo-Aral, T.F. Moura, A. Casini, G. Soveral, M. Echevarría, Functional inhibition of aquaporin-3 with a gold-based compound induces blockage of cell proliferation, J. Cell. Physiol. 229(11) (2014) 1787-801.

[33] X. Liu, Q. Zhang, Z. Hong, D. Xu, Induction of heartwood formation in young Indian sandalwood (Santalum album L.) by gas elicitors, Front Plant Sci 13 (2022) 961391.

[34] N.J. Khound, R.K. Bharali, Biosorption of fluoride from aqueous medium by Indian sandalwood (Santalum Album) leaf powder, Journal of Environmental Chemical Engineering 6(2) (2018) 1726-1735.

[35] S. Santha, C. Dwivedi, Anticancer Effects of Sandalwood (Santalum album), Anticancer Res. 35(6) (2015) 3137-45.

[36] R.L. Moy, C. Levenson, Sandalwood Album Oil as a Botanical Therapeutic in Dermatology, J. Clin. Aesthet. Dermatol. 10(10) (2017) 34-39.

[37] C. Ortiz, L. Morales, M. Sastre, W.E. Haskins, J. Matta, Cytotoxicity and Genotoxicity Assessment of Sandalwood Essential Oil in Human Breast Cell Lines MCF-7 and MCF-10A, Evid. Based Complement. Alternat. Med. 2016 (2016) 3696232.

[38] A. Bommareddy, J. Oberlin, K. Blankenhorn, S. Hughes, E. Mabry, A. Knopp, A. VanWert, C. Dwivedi, I. Pinkerton, L. Gutierrez, Alpha-santalol, a derivative of sandalwood oil prevents development of prostate cancer in TRAMP mice, Phytomedicine Plus 4(1) (2024) 100523.

[39] K. Vermeulen, D.R. Van Bockstaele, Z.N. Berneman, The cell cycle: a review of regulation, deregulation and therapeutic targets in cancer, Cell Prolif. 36(3) (2003) 131-49.

[40] L. Li, X. Chen, H. Gu, The signaling involved in autophagy machinery in keratinocytes and therapeutic approaches for skin diseases, Oncotarget 7(31) (2016) 50682-50697.

[41] X. Li, H.L. Xu, Y.X. Liu, N. An, S. Zhao, J.K. Bao, Autophagy modulation as a target for anticancer drug discovery, Acta Pharmacol. Sin. 34(5) (2013) 612-24.

[42] 42. S.E. Dickinson, E.R. Olson, C. Levenson, J. Janda, J.J. Rusche, D.S. Alberts, G.T. Bowden, A novel chemopreventive mechanism for a traditional

medicine: East Indian sandalwood oil induces autophagy and cell death in proliferating keratinocytes, Arch. Biochem. Biophys. 558 (2014) 143-52.

[43] S. Ijaz, N. Akhtar, M.S. Khan, A. Hameed, M. Irfan, M.A. Arshad, S. Ali, M. Asrar, Plant derived anticancer agents: A green approach towards skin cancers, Biomed. Pharmacother. 103 (2018) 1643-1651.

[44] K. Singh, H. Maurya, P. Singh, P. Panda, AK Behera, A. Jamal, G. Eslavath, S. Mohapatra, H. Chauhan, D. Sharma, DISPEL: database for ascertaining the best medicinal plants to cure human diseases, Database (Oxford) 2023 (2023).

[45] R.P. Vivek-Ananth, K. Mohanraj, A.K. Sahoo, A. Samal, IMPPAT 2.0: An Enhanced and Expanded Phytochemical Atlas of Indian Medicinal Plants, ACS Omega 8(9) (2023) 8827-8845.

[46] 46. T. Schwede, J. Kopp, N. Guex, M.C. Peitsch, SWISS-MODEL: An automated protein homology-modeling server, Nucleic Acids Res. 31(13) (2003) 3381-5.

[47] G. Studer, G. Tauriello, S. Bienert, M. Biasini, N. Johner, T. Schwede, ProMod3-A versatile homology modelling toolbox, PLoS Comput. Biol. 17(1) (2021) e1008667.

[48] J. Xu, F. Jiao, B. Berger, A tree-decomposition approach to protein structure prediction, Proc IEEE Comput Syst Bioinform Conf (2005) 247-56.

[49] G.G. Krivov, M.V. Shapovalov, R.L. Dunbrack, Jr., Improved prediction of protein side-chain conformations with SCWRL4, Proteins 77(4) (2009) 778-95.

[50] P. Eastman, J. Swails, J.D. Chodera, R.T. McGibbon, Y. Zhao, K.A. Beauchamp, L.P. Wang, A.C. Simmonett, M.P. Harrigan, C.D. Stern, R.P. Wiewiora, B.R. Brooks, V.S. Pande, OpenMM 7: Rapid development of high performance algorithms for molecular dynamics, PLoS Comput. Biol. 13(7) (2017) e1005659.

[51] A.D. Mackerell, Jr., M. Feig, C.L. Brooks, 3rd, Extending the treatment of backbone energetics in protein force fields: limitations of gas-phase quantum mechanics in reproducing protein conformational distributions in molecular dynamics simulations, J. Comput. Chem. 25(11) (2004) 1400-15.

[52] V.B. Chen, W.B. Arendall, 3rd, J.J. Headd, D.A. Keedy, R.M. Immormino, G.J. Kapral, L.W. Murray, J.S. Richardson, D.C. Richardson, MolProbity: all-atom structure validation for macromolecular crystallography, Acta Crystallogr. D Biol. Crystallogr. 66(Pt 1) (2010) 12-21.

[53] P. Benkert, M. Biasini, T. Schwede, Toward the estimation of the absolute quality of individual protein structure models, Bioinformatics 27(3) (2011) 343-50. https://doi.org/10.1093/bioinformatics/btq662.

[54] E.F. Pettersen, T.D. Goddard, C.C. Huang, G.S. Couch, D.M. Greenblatt, E.C. Meng, T.E. Ferrin, UCSF Chimera--a visualization system for exploratory research and analysis, J. Comput. Chem. 25(13) (2004) 1605-12.

[55] O. Trott, A.J. Olson, AutoDock Vina: improving the speed and accuracy of docking with a new scoring function, efficient optimization, and multithreading, J. Comput. Chem. 31(2) (2010) 455-61.

[56] S. Dallakyan, A.J. Olson, Small-molecule library screening by docking with PyRx, Methods Mol. Biol. 1263 (2015) 243-50.

[57] Discovery Studio Modeling Environment, Release 4.5. 2021. BIOVIA, Dassault Systèmes, San Diego.

[58] A. Daina, O. Michielin, V. Zoete, SwissADME: a free web tool to evaluate pharmacokinetics, drug-likeness and medicinal chemistry friendliness of small molecules, Sci. Rep. 7(1) (2017) 42717.

[59] 59. C.A. Lipinski, F. Lombardo, B.W. Dominy, P.J. Feeney, Experimental and computational approaches to estimate solubility and permeability in drug discovery and development settings, Adv Drug Deliv Rev 46(1-3) (2001) 3-26.

[60] D.A. Filimonov, A.A. Lagunin, T.A. Gloriozova, A.V. Rudik, D.S. Druzhilovskii, P.V. Pogodin, V.V. Poroikov, Prediction of the Biological Activity Spectra of Organic Compounds Using the Pass Online Web Resource, Chemistry of Heterocyclic Compounds 50(3) (2014) 444-457.

[61] G. Xiong, Z. Wu, J. Yi, L. Fu, Z. Yang, C. Hsieh, M. Yin, X. Zeng, C. Wu, A. Lu, X. Chen, T. Hou, D.

Cao, ADMETlab 2.0: an integrated online platform for accurate and comprehensive predictions of ADMET properties, Nucleic Acids Res. 49(W1) (2021) W5-w14.

[62] C. Oostenbrink, A. Villa, A.E. Mark, W.F. van Gunsteren, A biomolecular force field based on the free enthalpy of hydration and solvation: the GROMOS force-field parameter sets 53A5 and 53A6, J. Comput. Chem. 25(13) (2004) 1656-76.

[63] M.J. Abraham, T. Murtola, R. Schulz, S. Páll, J.C. Smith, B. Hess, E. Lindahl, GROMACS: High performance molecular simulations through multi-level parallelism from laptops to supercomputers, SoftwareX 1-2 (2015) 19-25.

[64] P. Bjelkmar, P. Larsson, M.A. Cuendet, B. Hess, E. Lindahl, Implementation of the CHARMM Force Field in GROMACS: Analysis of Protein Stability Effects from Correction Maps, Virtual Interaction Sites, and Water Models, J. Chem. Theory Comput. 6(2) (2010) 459-66.